Unraveling Intermolecular VWFA1-GP1bα and VWF C4-GP2b3a Interactions Using Atomic Force Microscopy

Unraveling Intermolecular VWFA1-GPIbα and VWF C4-GP2b3a Interactions Using Atomic Force Microscopy

A Thesis Presented

By

Sherly Fadel Makar

Submitted to the Graduate School of the University of Massachusetts Amherst in partial fulfillment of the requirements for the degree of

Master of Science

February 2024

Biomedical Engineering

Unraveling Intermolecular VWFA1-GPIbα and VWF C4-GP2b3a Interactions Using Atomic Force Microscopy

A Thesis Presented

By

Sherly Fadel Makar

Approved as to style and content by:

X. Frank Zhang, Chair

S. Thai Thayumanavan, Department Head
Department of Biomedical Engineering

ABSTRACT

UNRAVELING INTERMOLECULAR VWFA1-GPIBA AND VWF C4-GP2B3A INTERACTIONS USING ATOMIC FORCE MICROSCOPY

FEBRUARY 2024

SHERLY FADEL MAKAR, B.A., UNIVERSITY OF ARKANSAS

M.S., UNIVERSITY OF MASSACHUSETTS AMHERST

Directed by: Professor X. Frank Zhang

Von Willebrand factor (VWF) is one of the largest and most complex glycoproteins. It is the main player in maintaining hemostasis at injury sites in the blood vessels as it bridges the interaction between blood platelets and the extracellular matrix (ECM). VWF acts as a mechanosensor in high-shear surroundings, leading to a conformational change in its domains. VWF is a mosaic protein with many different domains that are receptors to the proper ligands on the blood platelets. The A1 domain is the initial point of contact between the VWF and the blood platelets as it binds to the glycoprotein 1b- α (GPIbα), followed by the binding between the C4 domain and the GP2b3a.

Intermolecular interactions between the A1 domain and the surrounding mucin-like linkers modulate the interaction between the A1 and the GPIb-α. Here, we present the effect of C- and the N-linkers on the A1 vs. GPIb- α interactions. Using atomic force microscopy, we proved that removing the sialic acid in the AIM enhances the binding frequency, strengthens the bond, and changes its conformation. We also verified that botrocetin hinders the effect of the AIM on this binding. We demonstrated that N-linked

glycans in the A2 domain affect the stability of the bond by decreasing the bond strength, although it increases the binding frequency when using the A1A2A3 fragment. In contrast, the sialic acid in the C-linker does not affect the binding frequency but decreases the bond strength.

The interaction between the C4 domain and the GP2b3a is the final step to ensure the formation of the platelet plug in bleeding. We proved that the bond formed is affected by the arginine-glycine-aspartic (RGD) sequence near the GP2b3a binding site in the C4 domain. The point mutations in the RGD sequence (F2561T &F2561S) enhance the conformation change of the VWF by exposing the GP2b3a binding epitope in the C4 domain, leading to increasing the binding frequency between the C4 in a VWF dimer and the GP2b3a.

TABLE OF CONTENTS

Page

LIST OF TABLES

LIST OF FIGURES

Figure Page

CHAPTER 1

INTRODUCTION

1.1 The role of the von Willebrand Factor in maintaining hemostasis.

The von Willebrand factor (VWF) is one of the largest and the most complex glycoproteins with 2050-residue monomers linked head-to-head and tail-to-tail into concatemers up to 200 monomers in length [1], [2]. Under native resting conditions, VWF is globular and coiled with strong intra- and intermolecular forces masking the binding sites. Whenever there is an injury in the blood vessels, high shear force induces a conformational change to the VWF, altering it into an elongated thread-like adhesive glycoprotein and exposing all the binding sites to the proper ligands, as shown in Figure 1.1 [3]. At the injury sites, VWF cross-links the extracellular matrix (ECM) of subendothelial cells with blood platelets [4]. VWF is a mosaic protein with each domain having its proper ligand to maintain homeostasis and form the blood plug [5].

Hemostasis is initiated when VWF multimers unfold at the A2 domain under elevated shear stress, followed by the interaction between the A3 domain and matrix collagen I-III, as demonstrated in Figure 1.1. This induces a conformational change in the A1 domain, initiating the initial platelet interaction and activation as the A1 domain binds to the glycoprotein 1bα (GPIbα). This interaction stimulates calcium release, subsequent platelet activation, inside-out signaling, and subsequent conformational change of the fibrinogen receptor (GPIIb/IIIa), which binds to the C4 domain in the VWF to favor the platelet plug formation [6], [7], [8].

The initial interaction between VWF and blood platelets occurs between the A1 domain and the glycoprotein 1bα (GPIbα), the largest subunit of the GPIb-IX complex

with a mass of 135 kDa [9], [10]. GPIbα is a heterodimer glycoprotein with α & β chains linked by disulfide bonds. GPIbα is highly glycosylated with 48 O-linked glycans and 1 N-linked glycan [11]. These glycans are diverse, including sialoglycans, Tn antigen, T antigen, and ABO(H) antigens. Additionally, they have been implicated as antigens in platelet clearance, von Willebrand factor binding, and immune thrombocytopenia syndromes.

1.2 A1 domain and its intramolecular interactions with the surrounding domains

Among all VWF domains, the A1 domain is unique in separated from D`D3 and A2 by O-glycosylated mucin-like segments: N-linker and C-linker, respectively [12]. It has been proposed that these linkers form autoinhibitory modules (AIMs) that might mask the GPIbα binding epitope under static conditions. High shear hydrodynamic force is transmitted through the linkers, exposing this binding site and initiating platelet arrest at sites of vascular injury. Using electron microscopy, it has been proved that when subjected to tensile forces, the central region of A1, spanning from residues 1273 to 1457, remains shielded from complete unwinding. However, the impact of mechanical strain is primarily borne by the segments of A1 positioned outside the disulfide linkage, encompassing residues 1238 to 1272 and 1458 to 1489; thus, the stability of internal residues is expected to be affected by the elongation of external residues by tensile force. Several studies have demonstrated that AIM affects A1 thermostability and the binding affinity between A1 and GPIbα [12] , [13] , [14]. In addition, it has been proven that the deletion of any of the AIM segments, type 2B VWD mutation, and ristocetin treatment leads to a decrease in the AIM mechanical stability and a heightened in the A1 and GPIbα binding [15]. As a result of an increase in the HDX of N-AIM (N-linker) residues

and AIM disintegration, Deng et al. speculate that ristocetin binds directly to C-AIM and disrupts the crosstalk between C-AIM and N-AIM [15], [13]. Using biomembrane force probe (BFP) assays, the N-linker has been implicated in the catch-bond behavior as the force first decelerated and then accelerated (slipped) the dissociation [16]. With these results in hand, the kinetic details of the A1-GPIbα interactions and the effect of the AIM on such binding remain a puzzle that requires further research to unravel.

Of note, many sporadic observations have proven the interrelation between the A1 and A2 domains in VWF. One study proposes that the A1 domain inhibits the force-regulated cleavage of the A2 domain by ADAMTS13 and that binding the A1 with the GPIbα relieves this inhibition [17]. In another study, the removal of the A2 domain leads to an increase in A1 vs. GPIbα binding in the presence of ristocetin. Additionally, during inflammation in sickle cell disease, it has been noted that methionine oxidation in the A1, A2, &A3 leads to VWF pro-thrombotic effects [18]. In the same study, MD simulations and dynamic flow assay have indicated that methionine oxidation removes the inhibitory effect of the A2 by destabilizing the binding interface between the A1 and A2 domains, thereby exposing the GpIbα-binding site within the A1 domain. Literature from previous studies collectively has raised the hypothesis that crosstalk between the A1 & A2 domains regulates A1 and GPIbα binding. Given that glycans are essential for protein folding and stability in general and modulating VWF structure (20% of VWF monomeric mass), function, and half-life in particular, changes in the N-linked glycans in the A2 domain may modulate the access of GPIbα receptor on A1 domain [19].

It has been established that A2 N-linked glycans stabilized the A2 domain against unfolding. However, little is known about the role of A2 N-linked glycans in mediating the A1 vs. GPIbα interaction [20].

1.3 The effect of the C4 RGD sequence and the neighboring regions on the interaction with GP2b3A

RGD is an acidic protein sequence with an arginine-glycine-aspartic acid motif. RGD sequence serves as a binding point between proteins and cell surfaces with a high affinity to integrins [21], [22], [23]. RGD sequence is a cell attachment site for adhesive extracellular matrix, cell surface proteins, integrins, and blood components [24]. Synthetic peptides with RGD sequences can induce integrin-proteins binding only if they are presented on a cell surface, not when in a solution. Using molecular dynamics simulation methods, it has been proven that RGD length and temperature affect its binding with integrin receptors, the stability of this binding, and the conformation [25]. Drugs based on RGD structure are promising for treating thrombosis, inflammation, and cancer.

The C2 and the C4 domains in the VWF contain the RGD sequence that binds to the glycoprotein 2b3a (GP2b3a) presented on the blood platelets [22], [25]. Gp2b3a or integrin αIIbβ3 is a calcium-dependent heterodimer and is one of the most abundant platelet receptors [23]. In homeostasis, GP2b3a exhibits the lowest binding affinity to the VWF domains [23], [26], [27]. However, in bleeding and high blood flow, “inside-out signaling” activates GP2b3a by changing its conformation and changing its state to increased binding affinity to become a competent receptor for RGD-sequence containing plasma adhesive proteins such as VWF and form the blood plug. The binding of VWF to

activated platelet receptors depends on the presence of the RGD sequence residues at 1744-1746 [27]. Human umbilical vein endothelial cells (HUVECs) bind to VFW in an RGD-dependent manner. As reported by Dejana et al., VWF adhesion to human umbilical vein endothelial cells (HUVECs) can be inhibited with an antibody against Gly1737 to Ser1750 in the RGD sequence. However, this binding is unaffected by antibodies against neighboring residues in the VWF RGD sequence Gly 1740-Ser 1742. It has been proven that there might be a second adhesion site other than the RGD sequence on the VWF for the GP2b3a or the HUVEC to bind to.

Unlike other C domains in the VWF, the C4 domain has an unconventional disulfide bond [25]. The C4 domain has a loop with the RGD sequence that aligns with the unique disulfide bond. This complex makes the RGD motif more accessible to the GP2b3a binding. Mutations near the RGD sequence in the C4 domain yield a significant impact on VWF function [28], [25], [29]. For Instance, in the p.Phe2561Tyr variant, residues close to the RGD-binding sequence alter VWF behavior. It accelerates platelet aggregation at lower shear rates compared to the wild-type VWF. Another mutation, p.Pro2555Arg, also near the RGD motif in the C4 domain, increases platelet aggregation size. This means that platelets are more prone to clumping under certain flow conditions, leading to excessive blood clot formation.

These mutations near the RGD sequence emphasize the delicate balance in the VWF's structure and function. We can expect that unrelated changes in the amino acid sequence can affect how VWF interacts with platelets, resulting in bleeding disorders or abnormal blood clotting risks.

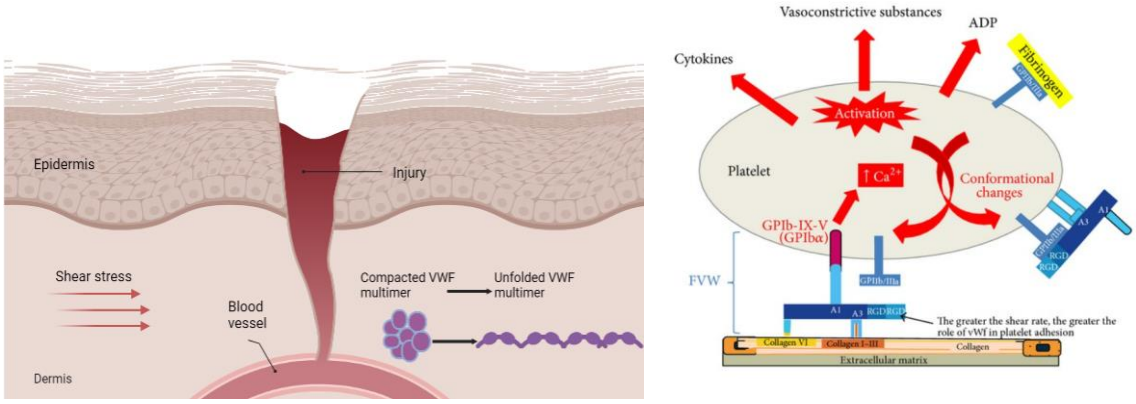

Figure 1.1 The role of VWF in hemostasis. (a) High shear stress at the sites of injury induces a conformational change in the VWF, exposing all the binding sites to their proper ligands. (b) A visual representation of maintaining homeostasis through the binding of different VWF domains to the proper ligands forming blood plugs, adopted from reference [7].

1.4 Thesis outline

Herein, the goal of the study in the 1st chapter is to pinpoint the interplay between A1 and the neighboring domains by studying their role in the binding kinetics between A1 and GPIbα using atomic force microscopy (AFM). AFM offers unprecedented capabilities in quantifying the biophysical interactions between molecules on a single particle level rather than an ensemble with piconewton force sensitivity. With all these advantages at hand, we will use the AFM to study the biophysical interactions between GPIbα and different VWF fragments: long A1 domain, A1A2A3 domain, and A3 domain. AFM results will uncover previously inconceivable quantitative insights into binding frequency, bond strength, and the conformation adopted by the A1 domain and GPIbα when bound in hemorrhage. This research will provide deep insights into the effect of sialic acid in the O-linked glycans in the AIM fragments and the N-linked glycans in the A2 domain on the binding strength and binding conformation between A1 and GPIbα.

Further exploration of these molecular interactions promises to present a seminal discovery to deeply understand the intermolecular interaction between different VWF

fragments to form the platelet plug and achieve the required balanced interaction between the A1 domain and GPIbα to avoid bleeding or thrombosis. This research will potentially pave the way to discover innovative therapies for disorders leading to excessive bleeding in case of fragments hindering A1 vs. GPIbα binding or thrombosis in case of fragments excessively enhancing such binding.

In collaboration with Dr. Tom McKinnon from the Imperial College, London, our study in the 2nd chapter investigated the impact of point mutations near the RGD sequence (Phe2561Thr, Phe2561Ser) on the biophysical interaction between the C4 domain in a VWF dimer and GP2b3a on the blood platelets using AFM with the RGG being used as a negative control. We examined the binding frequency, dissociation rates, and the energy barrier width induced by these mutations to determine whether they enhance the ligand-receptor bond strength and change the bond conformation between the C4 and the GP2b3a. This study aims to provide deeper insights into the kinetics of gain-of-function diseases such as arterial thrombosis, deep vein thrombosis (DVT), pulmonary embolism (PE), thrombotic microangiopathies, and Budd-Chiari syndrome.

CHAPTER 2

NEIGHBORING GLYCANS IN ADJACENT FRAGMENTS INFLUENCE A1 DOMAIN INTERACTIONS WITH GPIBα AT INJURY SITES

2.1. Experimental details

2.1.1. Protein validation

The long A1 domain we used has residues 1238-1481 with 5 O-linked glycans from the AIM region, while A1A2A3 residues 1261-1874 have the C-linker only from the AIM region. Both the long A1 and A1A2A3 were purchased from ImmunoPrecise, and the GPIbα platelet receptor was purchased from Sinobiological. α2-3,6,8,9 Neuraminidase A enzyme from New England Biolabs was used to catalyze the hydrolysis of all linear and branched non-reducing terminal sialic acid residues in the O-linked glycans and PNGase F from New England Biolabs was used to remove all N-linked glycans. All protein treatments with enzymes were done before protein immobilization on the amine-treated glass slide. Long A1 was treated with α2-3,6,8,9 Neuraminidase A enzyme for 1 hour at 37℃. A1A2A3 was treated with α2-3,6,8,9 Neuraminidase A enzyme and PNGase in non-denaturing conditions for 1 hour and 4 hours, respectively, at 37℃ separately. Long A1 was treated with the snake venom protein botrocetin 1:1 molar ratio for 30 minutes at 37℃ after the long A1 was immobilized on the amine-treated glass slide.

2.1.2 Cantilever preparation/coverslip preparation for single molecule force spectroscopy

Single-molecule experiments testing different VWF domains vs. GPIbα interactions were conducted using a home-built AFM to study biophysical interactions between molecules. MLCT-Bio-DC cantilevers were purchased from Bruker Nano. AFM- cantilever tips and glass slides amino-functionalization was achieved by APTES in the gas phase method according to the detailed protocol developed by Dr. Hermann J. Gruber of Johannes Kepler University https://www.jku.at/fileadmin/gruppen/216/03_AFM_tip_aminofunctionalization_2016_05_06.pdf [30]. Cantilever tips are pretreated using chloroform to remove contamination and add silanol groups (Si-OH) required for subsequent amino functionalization. Cantilever tips are then treated with (3-Aminopropyl) triethoxysilane (APTES) to introduce amine groups with the help of the catalyst triethylamine in a glass chamber filled with argon gas. After 48 hours, Acetal-PEG-NHS is used as a crosslinker between the amine group and the protein (added later). Citric acid is added to convert the acetal group into an aldehyde group. Finally, the protein is immobilized by attaching to the aldehyde group and adding ethanolamine to block any non-specific binding. Amine-treated glass slides were used, so we treated them starting from the Acetal-PEG-NHS. Protein immobilization is preferred to be done freshly on the same day of an experiment.

To ensure durability after multiple interactions between proteins, we have the more stable protein on the cantilever tip. That being said, 80 μL of 1μM GPIbα is immobilized on the cantilever tip, and 80 μL of 1μM of different VWF fragments are immobilized on the glass slide. The A3 domain is the negative control to establish the

baseline of low binding frequency. During the experiments, the compression force is kept within the range of 200-300pN to protect the proteins from denaturing. Data was collected at four different retraction speeds (0.94, 1.88, 3.76, and 7.52 μm/s) to calculate the rupture forces and loading rates. Each experiment has 10-15 points for each speed, and each point has 20-30 readings. All measurements were conducted at 25℃ in phosphate-buffered saline.

In this model, the spring constant was 0.012 N/m for all experiments, which agrees with the manufacturer's values (0.01 N/m). Rupture values and system springs were determined from each force curve, then rupture forces and loading rates were calculated.

2.2. Results

2.2.1. Specification of the binding of the long A1 domain with GPIbα

To quantify the binding affinity between the long A1 domain of residues 1238-1481 with 5 O-linked glycans and the platelet receptor GPIbα, we used the home-built AFM to get the binding frequency by lowering down the cantilever tip coated with GPIbα to bind with the long A1 domain immobilized on the glass slide then unbinding of the bond or rupture occurs when raising the GPIbα-coated cantilever tip to the initial position (aka piezo position). Figure 2.1 represents a single scan/reading showing the steps for an approach, and a retract between two molecules using AFM. The cantilever tip approaches the sample as the piezo moves down the base position (position 1). Then, the cantilever tip is in contact with the sample (1^{st} contact) (position 2). Position (3) is when the cantilever tip applies compression force on the sample, followed by position (4), during

which the cantilever tip starts to move up and unload the force. Finally, the cantilever tip completely detaches from the sample and moves back to the base position.

To study the effect of the sialic acids in the O-linked glycans within the AIM on the interactions between the A1 domain and GPIbα platelet receptor, we assessed the binding of both untreated-long A1 and the α2-3,6,8,9 Neuraminidase A -treated long A1 with GPIbα, using the A3 domain as a negative control (Fig. 2.2). Untreated long A1 has a binding frequency of 6.7%, which is not significant compared to the binding frequency of the A3 domain, which is non-specific (Fig. 2.2). On the other hand, α2-3,6,8,9 Neuraminidase A -treated long A1 has a binding frequency of 34.78% which is significantly different compared to that of the untreated long A1 (Fig. 2.2). Given that, α2-3,6,8,9 Neuraminidase A cleaves sialic acid residues from glycoproteins that are negatively charged, the repulsion between sialic acid negative charges and the negatively charged GPIbα hinders long A1. vs GPIbα binding.

With botrocetin treatment, we found that the binding frequency between the long A1 and the GPIbα is restored and increased to 36.68%, a significant increase over the untreated-long A1 (Fig. 2.2). Every approach and retract between different long A1 samples-treated glass slides and the GPIbα-treated cantilever tip is considered a binding and a rupture (unbinding) force between the two molecules, respectively which represents a single scan (Fig. 2.1). These unbinding forces (pN) were collected at different loading rates (pN/s) and different cantilever tip retraction speeds: 0.94, 1.88, 3.76, and 7.52 μm/s (piezo steps). To calculate the dissociation rate K^0 and the energetic barrier distance between the bond state and the transition state of the binding between different A1 samples and GPIbα (known as the energy barrier width, γ), the loading rates were

arranged ascendingly with their corresponding unbinding forces; then they were divided into 4 groups. The average loading rate (pN/s) for each group was calculated, and the most probable unbinding force (pN) was identified from histograms. Then, the average loading rates, along with their corresponding most probable unbinding forces, were plotted, as shown in Figure 2.3.

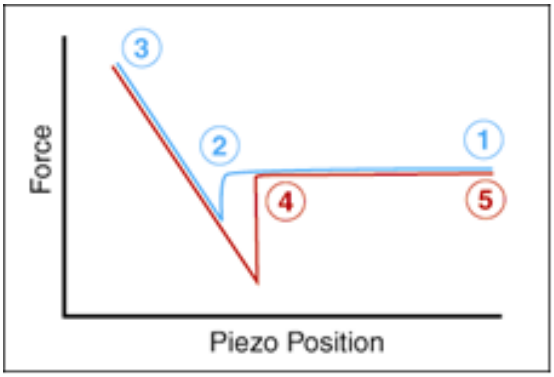

Figure 2.1 Hypothetical AFM force curves. The blue line is the approach trace, and the red line is the retract trace.

To determine the dissociation rate K^0 and the energy barrier width γ, the most probable unbinding forces with their corresponding loading rates were fitted to the Bell Evans model, as demonstrated in Table 2.1. From Table 2.1, there is a 3.78-fold difference when comparing the untreated-long A1 to Neuraminidase-treated long A1, proving that cleaving the negatively charged sialic acid in the O-linked glycans within the AIM strengthens the bond between the A1 domain and GPIbα platelet receptor.
The botrocetin-treated long A1 dissociation rate is 1.5-fold lower than that of the Neuraminidase-treated long A1, indicating a stronger bond between long A1 and GPIbα in the presence of botrocetin.

The third parameter we can get from conducting AFM experiments is the energy barrier width, which gives us some basic knowledge about the conformation these

molecules adopt when binding. Table 2.1 presents a 1.12-fold difference when comparing botrocetin-treated long A1 with Neuraminidase-treated long A1 and a 2.55-fold difference compared to the untreated long A1. In addition, neuraminidase-treated long A1 is 2.27-fold higher than untreated-long A1, similar to the difference between botrocetin-treated long A1 and untreated-long A1. Hence, we can say that the bond conformations of botrocetin- and Neuraminidase-treated long A1 are not the same, but the bond conformation is closer when comparing any of them to the untreated-long A1.

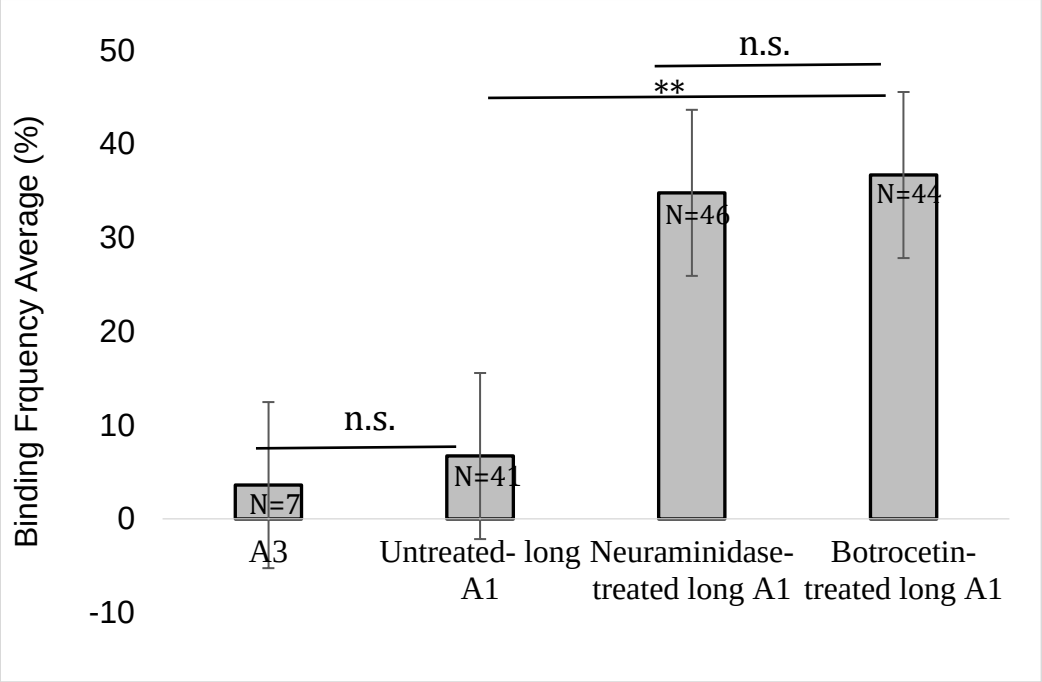

Figure 2.2 Binding frequencies of AFM experimental groups. Binding frequency averages for the untreated-long A1, Neuraminidase-treated long A1, and botrocetin-treated long A1. N denotes the sample number, n.s. Stands for non-significant, (**) corresponds to P<0.0001.

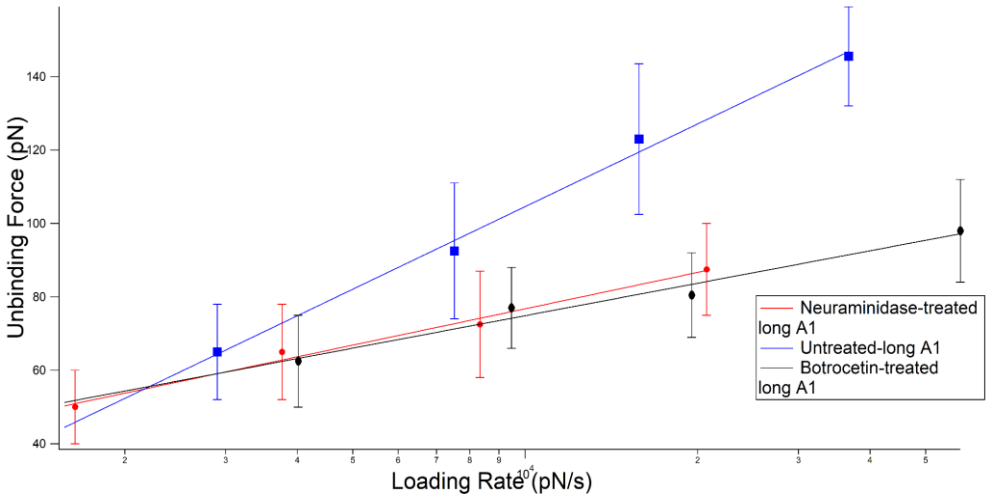

Figure 2.3 Dynamic force spectra of A1-GPIbα interactions. The dynamic force spectrum plots the most probable unbinding force (pN) vs. the loading rate (pN/s) after calculating the unbinding forces and the loading rates. The loading rates were arranged ascendingly with their corresponding unbinding forces and then were divided into 4 groups. The loading rate average is calculated for each group, and the unbinding forces are plotted in histograms. The center of the highest bin is the most probable unbinding force. The data are fitted to the Bell-Evans model to compute the dissociation rate and the energy barrier width. The red, blue, and black lines represent the binding between GPIbα and Neuraminidase-treated long A1, untreated-long A1, and botrocetin-treated long A1, respectively. The bars donate half of the bin width, representing the error in the calculated unbinding forces.

Table 2.1 The Dissociation rates K^0 and energy barrier widths γ computed from Bell-Evans fit in figure (2.3) using Igor analysis software.

Parameters/ VWF fragments	**Untreated-long A1**	**Neuraminidase-treated long A1**	**Botrocetin-treated long A1**
K^0: S^{-1}	12.288 ± 1.68	3.251 ± 0.982	2.2122 ± 1.41
γ: nm	0.1266 ± 0.00702	0.28767 ± 0.0221	0.32226 ± 0.0385

2.2.2. N-linked glycans and their impact on the A1 vs GPIbα binding.

To assess whether the N-linked glycans in the A2 domain influence the A1 vs GPIbα binding, we conducted AFM experiments to identify the binding specifications. The study involved untreated-A1A2A3 and PNGase-treated A1A2A3 with GPIbα, with A3 as a negative control. Cleaving N-linked glycans in the A2 domain using PNGase increases the binding frequency significantly compared to the untreated A1A2A3 and the negative control, as shown in Figure (2.4). These results indicate the N-linked glycans affect A1 vs. GPIbα binding on a single molecule level. Following the same analysis method mentioned in section 2.2.1 to generate Figure 2.5 and then fitting the average loading rates and their corresponding most probable unbinding forces, we computed the dissociation rate K^0 and the width of the energy barrier γ. Comparing the dissociation rates, PNGase-treated A1A2A3 is $\simeq$6-fold higher than the untreated-A1A2A3, indicating a weaker bond between the A1 domain and GPIbα when cleaving the N-linked glycans in the A2 as shown in Table 2.2. In addition to the dissociation rate K^0, there is a 1.32-fold difference in the energy barrier width γ implementing that PNGase-cleavage impacts the bond conformation adopted by the A1 and GPIbα when binding, as presented in Table 2.2.

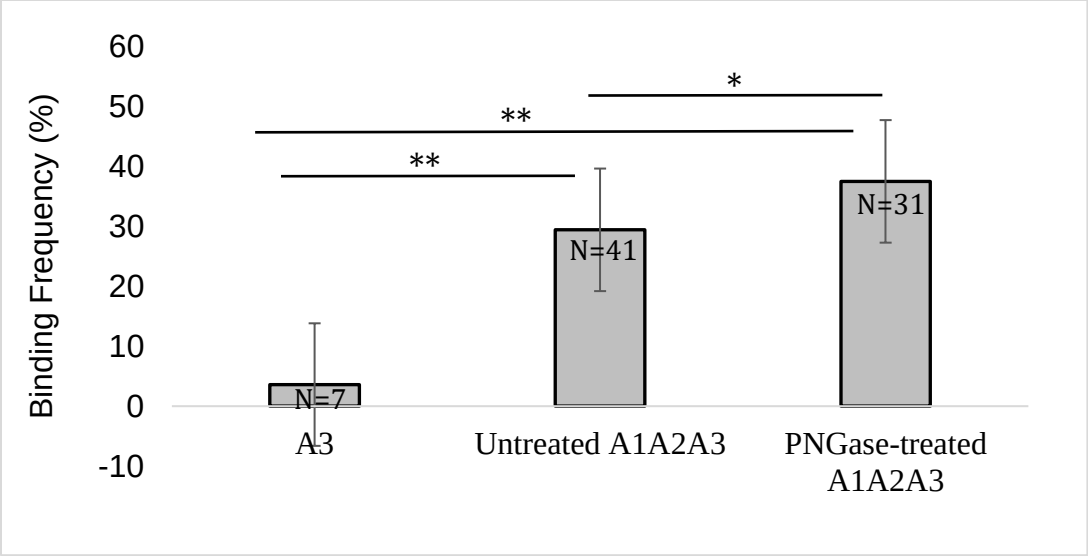

Figure 2.4 Binding frequencies of AFM experimental groups. Binding frequency averages for the untreated-long A1 and PNGase-treated A1A2A3. N denotes the sample number. (*) corresponds to P=0.0024 and (**) corresponds to P<0.0001.

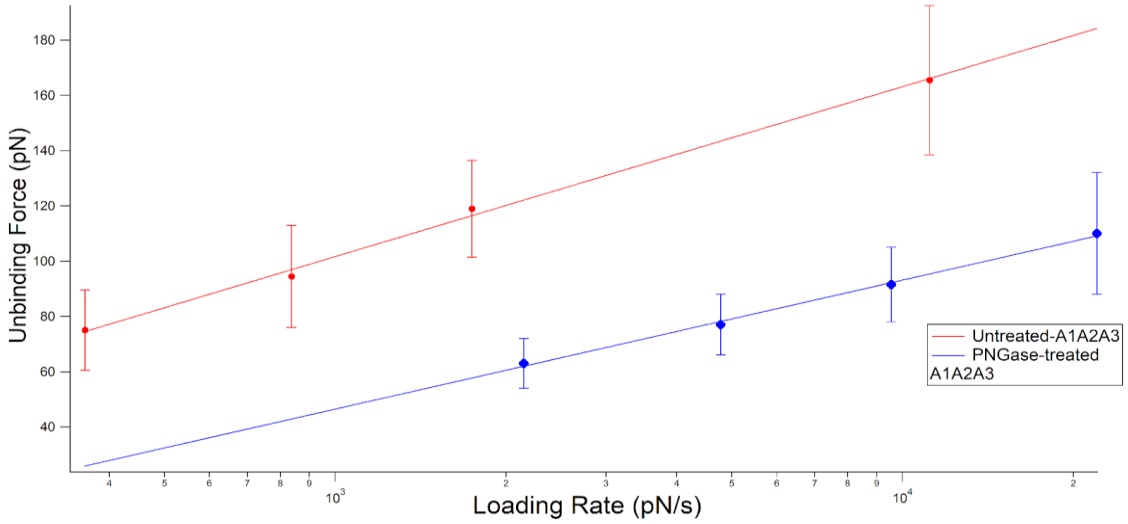

Figure 2.5 Dynamic force spectra of A1A2A3-GPIbα interactions. The dynamic force spectrum plots the most probable unbinding force (pN) vs. the loading rate (pN/s) that was calculated similarly to figure (2b) in section 3.2. The red and blue lines represent the binding between GPIbα and the untreated-A1A2A3 and the PNGase-treated A1A2A3, respectively. The bars represent half of the bin width, representing the error in the calculated unbinding forces.

Table 2.2 The Dissociation rates K^0 and energy barrier widths γ computed from Bell-Evans fit in figure (2.5) using Igor analysis software.

Parameters/ VWF fragments	Untreated-A1A2A3	PNGase-treated A1A2A3
K^0: S^{-1}	0.83234 ± 0.109	4.9874 ± 0.65
γ: nm	0.1539 ± 0.00578	0.20271 ± 0.00795

2.2.3. The impact of the O-linked glycans in the C-AIM on the A1 vs GPIbα binding.

To study whether the O-linked glycans in the C-linker solely between the A1 and the A2 domain affect the binding between A1 and GPIbα, we conducted AFM experiments using untreated-A1A2A3 and α2-3,6,8,9 Neuraminidase A treated-A1A2A3 vs. GPIbα. The A1A2A3 fragment we used in this experiment has residues 1261-1874, which have the C-AIM only and not the N-AIM. We calculated the binding frequency, the dissociation rate $K^{0,}$ and the energy barrier width γ the same way as explained earlier in section 3.1. The binding frequency does not differ significantly between the untreated-A1A2A3 and the α2-3,6,8,9 Neuraminidase A-treated A1A2A3 (Figure 2.6). Nevertheless, there is a 2.6-fold increase comparing the dissociation rate of α2-3,6,8,9 Neuraminidase A-treated A1A2A3 to untreated-A1A2A3 indicating a weakening in the bond strength when removing the sialic acid in the O-linked glycans in the C-AIM. Also, a 1.75-fold change in the energy barrier width suggests a change in the bond conformation when A1 binds to GPIbα upon removing the C-linker O-linked glycans, as demonstrated in Table 2.3.

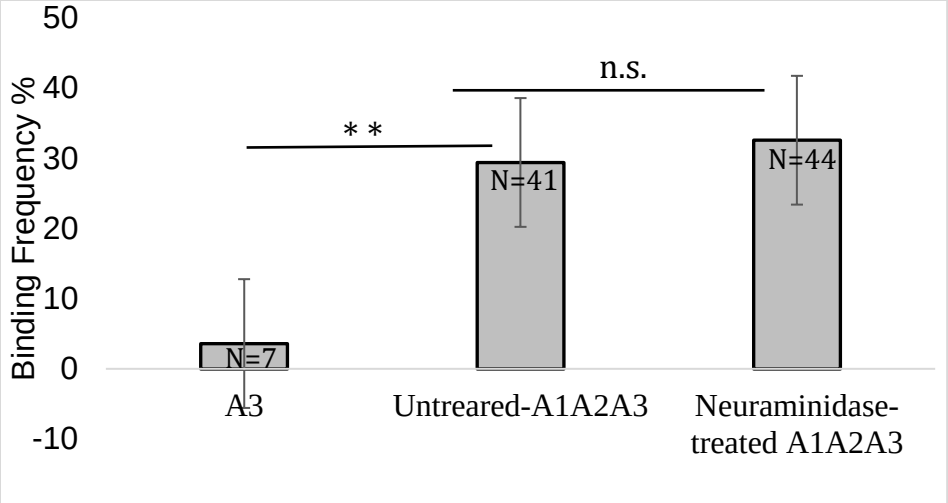

Figure 2.6 Binding frequencies of AFM experimental groups. Binding frequency averages for the untreated-A1A2A3 and Neuraminidase-treated A1A2A3. N denotes the sample number, n.s. stands for non-significant, and (**) corresponds to P<0.0001.

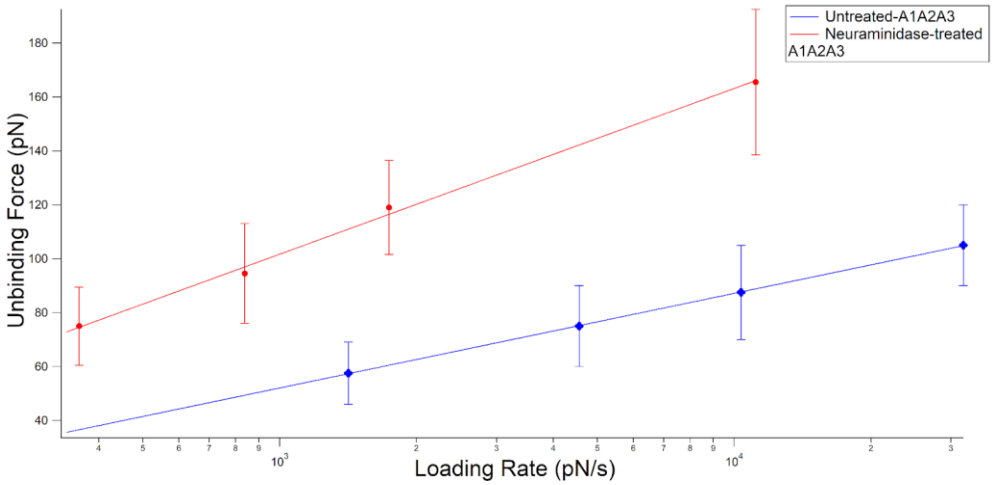

Figure 2.7 Dynamic force spectra of A1A2A3-GPIbα interactions. The dynamic force spectrum plots the most probable unbinding force (pN) vs. the loading rate (pN/s) that was calculated similarly to figure (2.5) in section 3.2. The blue and red lines represent the binding between GPIbα and the untreated-A1A2A3 and the Neuraminidase A-treated A1A2A3, respectively. The bars represent half of the bin width, representing the error in the calculated unbinding forces.

Table 2.3 The Dissociation rates K^0 and energy barrier widths γ computed from Bell-Evans fit in figure (4b) using Igor analysis software.

Parameters/ VWF fragmennts	Untreated-A1A2A32	Neuraminidase-treated A1A2A3
K^0: S^{-1}	0.83234 ± 0.109	2.1617 ± 0.0644
γ: nm	0.1539 ± 0.00578	0.26961 ± 0.00179

2.3. Discussion and future directions.

Among all the domains in the VWF, the A1 domain is uniquely special in being surrounded by the mucin-like linkers that affect A1 vs. GPIbα binding in hemorrhage. In addition to these linkers, it has been predicted that the A2 domain might impact this interaction; however, this impact has yet to be uncovered and studied in detail. Previous studies have used biolayer interferometry (BLI) and isothermal titration calorimetry (ITC) to study the association and the dissociation between the A1 and GPIbα and the thermodynamics of this interaction [12]. In this study, we used the AFM to study the biophysical interactions and the specifications of the A1 vs. GPIbα bond on a single molecule level, including the binding frequency, dissociation rate K^0, and the energetic barrier distance between the bond state and the transition state of the binding between different A1 samples and GPIbα. To conduct AFM experiments, we used GPIbα vs. long A1 residues from 1238 to 1481 with 5 O-linked glycans from the N-linker and most of the C-linker, A1A2A3 residues from 1261 to 1874 that have the C-linker and a very small portion from the N-linker, and A3 as a negative control. We used α2-3,6,8,9 Neuraminidase A enzyme to hydrolyze the O-linked glycans in the long A1 and A1A2A3, and we used PNGase to cleave the N-linked glycans in the A2 domain in the A1A2A3 fragment.

Our results proved that the O-linked glycans in the N and the C-linkers in the long A1 domain hinder the A1 vs. the GPIbα since Neuraminidase A -treated long A1 domain expressed a significantly higher binding frequency and lower dissociation rate compared to the untreated-long A1A2A3. Knowing that the dissociation rate is inversely proportional to the strength of the bond, a 3.78-fold decrease suggests a stronger bond is formed when removing the O-linked glycans. Additionally, a 2.27-fold difference in the energy barrier width indicates

a difference between the bonds' conformation created upon O-linked glycans removal in both linkers.

Botrocetin is a snake venom that is used as a universal induction for platelet aggregation between the GPIbα and the A1 domain [31], [32] , [33]. Botrocetin has been proven to enhance platelet agglutinating in an αIIbβ3-independent manner, unlike ristocetin [32]. This mechanism happens in a two-step reaction; the VWF-botrocetin complex is formed initially, forming a new interface that binds to the GPIbα [31], [33]. Based on our results, botrocetin treatment compensates for the presence of the O-linked glycans in the long A1 fragment and yields non-significant binding frequency compared to the long A1 treated with Neuraminidase-A1. However, botrocetin-treated long A1 resulted in a stronger bond between A1 and GPIbα. The difference in the energy barrier width confirms that botrocetin treatment regulates the VWF activity allosterically by changing the structure of the GPIbα binding surface on the A1. This observation aligns with the existing [33].

To determine the effect of the O-linked glycans in the C-linker in the presence of the A2 domain, we compared untreated-A1A2A3 with Neuraminidase A-treated A1A2A3. It is worth noting that the dissociation rate between the untreated-A1A2A3 and GPIbα is the lowest compared to any of the treated A1A2A3 samples or treated A1 samples, suggesting it has the strongest bond. However, untreated-A1A2A3 does not express the highest binding frequency. This conveys the pivotal role of the neighboring A2 and the C-linker in the A1 vs. GPIbα interaction, especially in exposing the GPIbα binding site in the A1 domain, increasing the binding frequency. The results can also imply that the A2 domain and/or the C-linker might have an impact on maintaining the stability of the bond as their presence yields the strongest bond compared to other experiments conducted. The binding strength might be related to the

stability of the A1 and GPIbα complex upon binding or the stability of the A1 domain when being exposed for the binding.

Upon hydrolyzing the sialic acid in the O-linked glycans in the C-linker, the binding frequency did not differ drastically from the untreated A1A2A3. However, a 2.6-fold increase in the dissociation rate substantiates a decrease in the A1 vs. GPIbα bond strength. This decrease can be due to a decrease in the stability of the A1 domain when removing the negative charge in the C-linker O-linked glycans. Additionally, a change in the energy barrier width indicates alterations in the force required for the dissociation of A1A2A3 from GPIbα, further supporting the idea that the C-linker O-linked glycans play a role in the stability of the interaction.

It is worth observing that the A1 vs. GPIbα bond is the strongest in the presence of the A1A2A3 full fragment, including the C-linker, which points out that the bond stability might be dependent on the presence of the C-linker, the A2, or the A3 domain or the presence of these three elements work cooperatively to stabilize the A1 vs GPIbα complex.

Literature has proved the crosstalk between A1 and A2 domains. For example, it has been proved that the A1 domain protects the A2 domain from ADAMTs13 cleavage, and this inhibition is released upon A1 vs. GPIbα interaction [34]. It has also been suggested that A2 domain deletion enhanced the binding between the A1 and GPIbα in the presence of ristocetin [17]. Martin et al. demonstrated that the isolated A2 domain binds to activated A1 domain polypeptide by immobilization or modulator, or the VWF, which dramatically decreases the arrested platelets in high shear conditions. Additionally, A1 and A2 domains will unfold simultaneously when exposed to urea [35]. With all these results in hand, we can conclude that A2 is an essential element in forming the A1 vs. GPIbα bond and the stability of this bond.

We cleaved the N-linked glycan in the A2 domain to uncover its importance in the A1 vs. GPIbα bond strength and stability. Although the binding frequency increased drastically when cleaving the N-linked glycans in the A2 domain in A1A2A3, the dissociation rate increased significantly, implying a decrease in the bond strength. These results convey the pivotal role of the N-linked glycans in the A2 domain in the A1 vs. GPIbα. The presence of the N-linked glycans in the A2 domain might be hindering this interaction by burying the GPIbα binding epitope in the A1 domain. However, their existence is crucial for the stability of the A1 domain, which is why their removal leads to the weakening of this bond.

In addition to the N-linked glycans, the A2 domain has a vicinal disulfide bond and calcium binding site (CBS) that have been proven to stabilize the A2 domain against unfolding and, therefore, protect it from ADAMTS13 cleavage using thermal unfolding and solution binding assays [20] , [36]. It would be worth investigating their effects on the A1 vs. GPIbα, whether they enhance or hinder the binding and the strength of the binding as well. A future direction that might be interesting to delve into is to study the effect of the vicinal disulfide bond, N-linked glycans, and the CBS on the catch-slip bond that is formed upon A1 vs. GPIbα binding to help us gain an in-depth understanding of the gain of function in VWD type 2B. Additionally, the effect of the N-linked glycans on the strength of the A1 vs. GPIbα might be related to the formation of the filopodia and lamellipodia, which is worth analyzing [37], [38], [39], [40].

CHAPTER 3

THE ROLE OF THE RGD NEIGHBORING SEQUENCE ON C4 VS. GP2B3A BINDING

3.1. Experimental details

The tips were prepared the same way detailed in Chapter 2 using the APTES in the gas phase method according to the detailed protocol developed by Dr. Hermann J. Gruber of Johannes Kepler University https://www.jku.at/fileadmin/gruppen/216/03_AFM_tip_aminofunctionalization_2016_05_06.pdf [30].

We immobilized 80 µl of 1µM GP2b3a on the cantilever tip and 80 µl of 0.4 µM VWF dimer on the glass slides. The glass slide was immersed in a low-binding affinity buffer of 1 mM Ca^{2+}, 1 mM Mg^{2+}, and 150 mM NaCl to activate the GP2b3a.

3.2. Results and discussion

The analysis was done exactly as detailed in Chapter 2 using Igor software to create histograms. Then, the Bell-Evans fit was used to calculate the dissociation rate and the energy barrier width.

To understand the effect of the neighboring regions to RGD sequence on the C4 vs. GP2b3a binding, we used the AFM to study the interaction between two mutated VWF dimers vs. GP2b3a, using the WT dimer as a positive control and the RGG sequence as a negative control. The two mutated VWF dimers have point mutations near the RGD sequence F2561T (Phe2561Thr) and F2561S (Phe2561Ser). We meticulously analyzed the binding frequency induced by these mutations on a single-molecule level using the AFM. We observed a significant difference in the binding frequency comparing

the F2561S to the WT (P=0.0063), and there is a more significant difference between the WT and the F2561T (P<0.0001) in the binding frequency, as shown in Figure 3.1. Also, it has been demonstrated that F2561T leads to higher binding with GP2b3a compared to the F2561S (P=0.0172), as presented in Figure 3.1.

Since the VWF we used to conduct these experiments is a dimer with two C4 domains, the binding frequencies shown in Figure 3.1 for the two mutants (F2561S and F2561T) could be between more than two molecules, mainly because the frequency is significant>30%. To ensure single-molecule interactions and to unveil the mechanism adopted by these mutations in modulating C4 vs. GP2B3a binding, we normalized the binding frequency by decreasing the concentration of the GP2b3a to half the concentration we used in Figure 3.1 experiments when interacting with F2561S and F2561Tto reach a binding frequency of 30% (the WT experiment was not normalized since we got ~30% binding frequency). When decreasing the GP2b3a concentration to 0.5μM, the binding frequencies decreased to 28 and 27 % for F2561S and F2561T, respectively. There is no significant difference comparing these binding frequencies to each other or to that of the WT (31.2 %).

From the combined Bell Evans fit presented in Figure 3.2, we computed the dissociation rate and the energy barrier width, as shown in Table 3.1, to gain a deeper understanding of the mechanism introduced by these point mutations in modulating the C4 vs. GP2b3a interaction in bleeding and injury. The WT dissociation rate is 65-fold higher than that of the F2561T and 3,364-fold higher than that of the F2561S. The decrease in the dissociation rate in the F2561S and the F2561S VWF-dimer is interpreted as a stronger bond formed between the C4 domain and the GP2b3a compared to the WT

dimer. These significant differences between the WT-VWF dimer and any of the two mutants after normalizing the binding frequency to 30% indicate that these point mutations enhance the binding between the C4 domain and the GP2b3a by opening up the VWF glycoprotein and exposing the GP2b3a binding epitope in the C4 domain resulting in a significantly stronger bond between the two molecules. A proposed mechanism for such an effect is that these point mutations in the amino acid sequence decrease the intramolecular forces between the VWF domains and induce a change in the coiled conformation of the VWF into extended glycoprotein. The F2561T dissociation rate is 54-fold higher than that of the F2561S, which indicates a stronger bond between the C4 and the GP2b3a in the latter.

The energy barrier width of the F2561T and F2561S is ~ 0.4, which suggests the conformation of the bond formed between the C4 and the GP2b3a is similar when replacing the phenylalanine with threonine or serine. This implies a similar effect caused by the threonine and serine mutations, and the difference might just be the strength of the intermolecular forces these amino acids diminish to expose the GP2b3a binding site in the C4 domain. However, the 4-fold difference comparing the energy barrier of the WT to that of any of the two mutants indicates a change in the bond conformation.

We can conclude that mutations near the RGD sequence in the C4 domain are a gain of function enhancing the binding between VWF and blood platelets by exposing the binding site of GP2b3a in the C4-VWF.

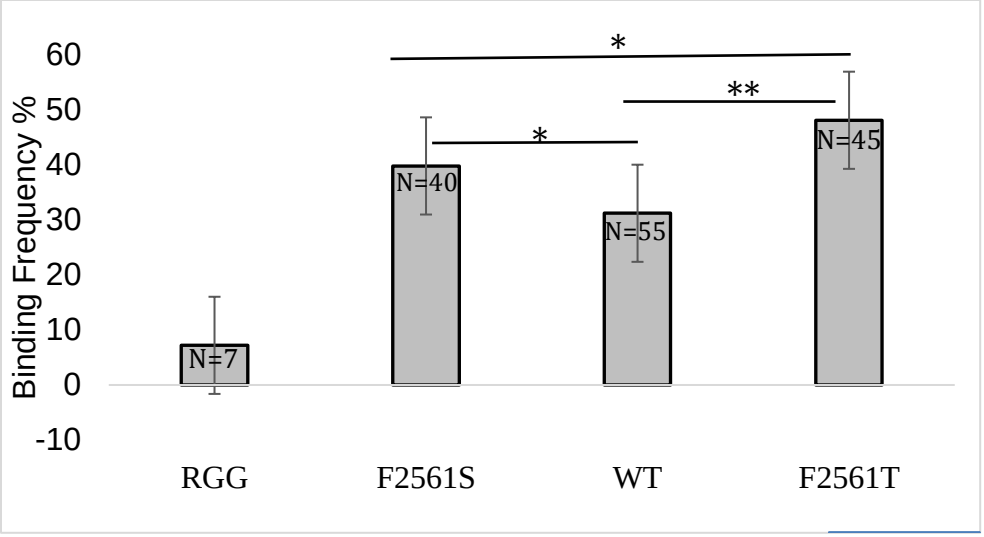

Figure 3.1 Binding frequencies of AFM experimental groups. Binding frequency averages for negative control RGG, the WT-VWF dimer, and the mutated VWF dimers near the RGD sequence: F2561T & F2561S. N denotes the sample number. (*) corresponds to P=0.0024 and (**) corresponds to P<0.0001. P =0.0172 comparing for F2561S &F2561T. P=0.0063 comparing the WT & F2561S.

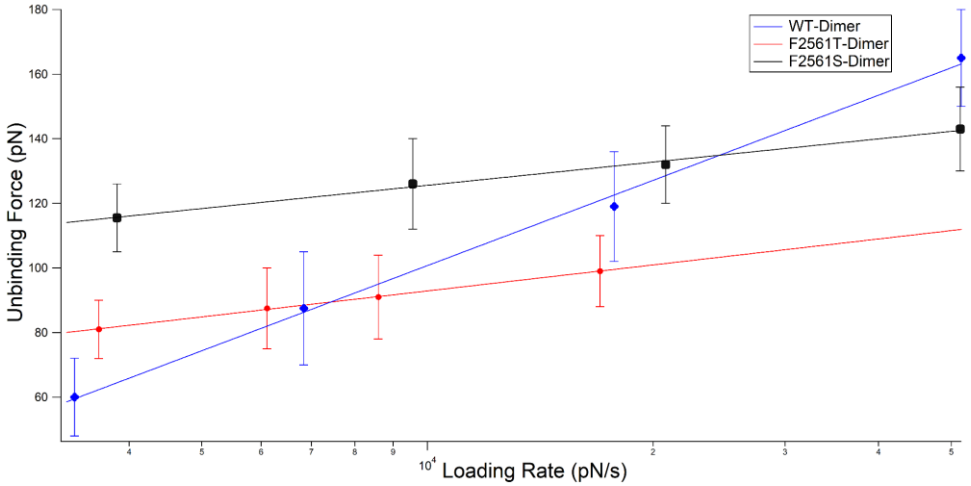

Figure 3.2 Dynamic force spectra of VWF- GP2b3a interactions. The dynamic force spectrum plots the most probable unbinding force (pN) vs. the loading rate (pN/s) that was calculated similarly to Chapter (1). The blue, red line, & black lines represent the binding between GP2b3a and the WT-dimer, F2561T-dimer, and F2561S-dimer, respectively. The bars represent half of the bin width, representing the error in the calculated unbinding forces.

Table 3.1 The Dissociation rates K^0 and energy barrier widths γ computed from Bell-Evans fit in figure (3.2) using Igor analysis software.

Parameters/ VWF dimers	**WT**	**F2561T**	**F2561S**
K^0: S^{-1}	18.614 ± 1.5	0.288±0.0425	0.005 ± 0.00337
γ: nm	0.10804 ± 0.00414	0.35±0.00774	0.396 ± 0.0218

BIBLIOGRAPHY

[1] E. T. Parker and P. Lollar, “Conformation of the von Willebrand factor/factor VIII complex in quasi-static flow,” *J Biol Chem*, vol. 296, p. 100420, Jan. 2021, doi: 10.1016/J.JBC.2021.100420.

[2] H. Fu, Y. Jiang, D. Yang, F. Scheiflinger, W. P. Wong, and T. A. Springer, “Flow-induced elongation of von Willebrand factor precedes tension-dependent activation,” *Nature Communications 2017 8:1*, vol. 8, no. 1, pp. 1–12, Aug. 2017, doi: 10.1038/s41467-017-00230-2.

[3] S. Okhota, I. Melnikov, Y. Avtaeva, S. Kozlov, and Z. Gabbasov, “Shear Stress-Induced Activation of von Willebrand Factor and Cardiovascular Pathology,” *Int J Mol Sci*, vol. 21, no. 20, pp. 1–18, Oct. 2020, doi: 10.3390/IJMS21207804.

[4] A. B. Federici, “The von Willebrand factor from basic mechanisms to clinical practice,” *Blood Transfusion*, vol. 9, no. Suppl 2, p. s1, 2011, doi: 10.2450/2011.001S.

[5] Y. F. Zhou, E. T. Eng, J. Zhu, C. Lu, T. Walz, and T. A. Springer, “Sequence and structure relationships within von Willebrand factor,” *Blood*, vol. 120, no. 2, p. 449, Jul. 2012, doi: 10.1182/BLOOD-2012-01-405134.

[6] G. A. Cortes, M. J. Moore, and S. El-Nakeep, “Physiology, Von Willebrand Factor,” *StatPearls*, Feb. 2023, Accessed: Dec. 25, 2023. [Online]. Available: https://www.ncbi.nlm.nih.gov/books/NBK559062/

[7] K. Ghoshal and M. Bhattacharyya, “Overview of platelet physiology: Its hemostatic and nonhemostatic role in disease pathogenesis,” *The Scientific World Journal*, vol. 2014, 2014, doi: 10.1155/2014/781857.

[8] G. König *et al.*, “Alteration in GPIIb/IIIa Binding of VWD-Associated von Willebrand Factor Variants with C-Terminal Missense Mutations,” *Thromb Haemost*, vol. 119, no. 7, pp. 1102–1111, 2019, doi: 10.1055/S-0039-1687878.

[9] M. Bryckaert, J. P. Rosa, C. V. Denis, and P. J. Lenting, “Of von Willebrand factor and platelets,” *Cellular and Molecular Life Sciences*, vol. 72, no. 2, pp. 307–326, Oct. 2015, doi: 10.1007/S00018-014-1743-8/FIGURES/5.

[10] G. Bendas and M. Schlesinger, “The GPIb-IX complex on platelets: insight into its novel physiological functions affecting immune surveillance, hepatic thrombopoietin generation, platelet clearance and its relevance for cancer development and metastasis,” *Experimental Hematology & Oncology 2022 11:1*, vol. 11, no. 1, pp. 1–22, Apr. 2022, doi: 10.1186/S40164-022-00273-2.

[11] M. A. Hollenhorst *et al.*, “Comprehensive analysis of platelet glycoprotein Ibα ectodomain glycosylation,” *J Thromb Haemost*, vol. 21, no. 4, p. 995, Apr. 2023, doi: 10.1016/J.JTHA.2023.01.009.

[12] K. Bonazza *et al.*, “Von Willebrand factor A1 domain stability and affinity for GPIbα are differentially regulated by its O-glycosylated N-and C-linker,” *Elife*, vol. 11, 2022, doi: 10.7554/ELIFE.75760.

[13] W. Deng *et al.*, “A discontinuous autoinhibitory module masks the A1 domain of von Willebrand factor,” *J Thromb Haemost*, vol. 15, no. 9, p. 1867, Sep. 2017, doi: 10.1111/JTH.13775.

[14] M. Auton, K. E. Sowa, M. Behymer, and M. A. Cruz, “N-terminal flanking region of A1 domain in von Willebrand factor stabilizes structure of A1A2A3 complex and modulates platelet activation under shear stress,” *J Biol Chem*, vol. 287, no. 18, pp. 14579–14585, Apr. 2012, doi: 10.1074/JBC.M112.348573.

[15] N. A. Arce *et al.*, “Activation of von Willebrand factor via mechanical unfolding of its discontinuous autoinhibitory module,” *Nat Commun*, vol. 12, no. 1, Dec. 2021, doi: 10.1038/S41467-021-22634-X.

[16] Y. C. Zhao, H. Wang, Y. Wang, J. Lou, and L. A. Ju, “The N-terminal autoinhibitory module of the A1 domain in von Willebrand factor stabilizes the mechanosensor catch bond,” *RSC Chem Biol*, vol. 3, no. 6, pp. 707–720, Jun. 2022, doi: 10.1039/D2CB00010E.

[17] C. Martin, L. D. Morales, and M. A. Cruz, “Purified A2 domain of von Willebrand factor binds to the active conformation of von Willebrand factor and blocks the interaction with platelet glycoprotein Ibα,” *Journal of Thrombosis and Haemostasis*, vol. 5, no. 7, pp. 1363–1370, Jul. 2007, doi: 10.1111/J.1538-7836.2007.02536.X.

[18] R. Tsai and G. Interlandi, “Oxidation shuts down an auto-inhibitory mechanism of von Willebrand factor,” *Proteins*, vol. 89, no. 6, p. 731, Jun. 2021, doi: 10.1002/PROT.26055.

[19] S. Ward, J. M. O’Sullivan, and J. S. O’Donnell, “The biological significance of von Willebrand factor o-linked glycosylation,” *Semin Thromb Hemost*, vol. 47, no. 7, pp. 855–861, Aug. 2021, doi: 10.1055/S-0041-1726373.

[20] C. J. Lynch and D. A. Lane, “N-linked glycan stabilization of the VWF A2 domain,” *Blood*, vol. 127, no. 13, p. 1711, Mar. 2016, doi: 10.1182/BLOOD-2015-09-672014.

[21] I. Vhora, S. Patil, P. Bhatt, and A. Misra, “Protein– and Peptide–Drug Conjugates: An Emerging Drug Delivery Technology,” *Adv Protein Chem Struct Biol*, vol. 98, pp. 1–55, Jan. 2015, doi: 10.1016/BS.APCSB.2014.11.001.

[22] H. Arzani, H. Rafii-Tabar, and F. Ramezani, “The investigation into the effect of the length of RGD peptides and temperature on the interaction with the αIIbβ3 integrin: a molecular dynamic study,” *J Biomol Struct Dyn*, vol. 40, no. 20, pp. 9701–9712, 2022, doi: 10.1080/07391102.2021.1932602.

[23] D. L. French and U. Seligsohn, “Platelet Glycoprotein IIb/IIIa Receptors and Glanzmann’s Thrombasthenia,” *Arterioscler Thromb Vasc Biol*, vol. 20, no. 3, pp. 607–610, 2000, doi: 10.1161/01.ATV.20.3.607.

[24] E. Ruoslahti, “RGD and other recognition sequences for integrins,” *Annu Rev Cell Dev Biol*, vol. 12, pp. 697–715, 1996, doi: 10.1146/ANNUREV.CELLBIO.12.1.697.

[25] E. R. Xu *et al.*, “Structure and dynamics of the platelet integrin-binding C4 domain of von Willebrand factor,” *Blood*, vol. 133, no. 4, p. 366, Jan. 2019, doi: 10.1182/BLOOD-2018-04-843615.

[26] J. J. Calvete, “Clues for understanding the structure and function of a prototypic human integrin: The platelet glycoprotein IIb/IIIa complex,” *Thromb Haemost*, vol. 72, no. 1, pp. 1–15, 1994, doi: 10.1055/S-0038-1648803/ID/JR_5/BIB.

[27] D. A. Beacham, R. J. Wise, S. M. Turci, and R. I. Handin$, “THE JOURNAL OF BIOLOGICAL CHEMISTRY Selective Inactivation of the Arg-Gly-Asp-Ser (RGDS) Binding Site in von Willebrand Factor by Site-directed Mutagenesis*,” *Journal of Biological Chemistry*, vol. 267, no. 5, pp. 3409–3415, 1992, doi: 10.1016/S0021-9258(19)50746-3.

[28] V. Huck *et al.*, “Gain-of-Function Variant p.Pro2555Arg of von Willebrand Factor Increases Aggregate Size through Altering Stem Dynamics,” *Thromb Haemost*, vol. 122, no. 2, p. 226, Feb. 2022, doi: 10.1055/A-1344-4405.

[29] R. Schneppenheim *et al.*, “The von Willebrand factor Tyr2561 allele is a gain-of-function variant and a risk factor for early myocardial infarction,” *Blood*, vol. 133, no. 4, pp. 356–365, Jan. 2019, doi: 10.1182/BLOOD-2018-04-843425.

[30] L. Wildling *et al.*, “Linking of sensor molecules with amino groups to amino-functionalized AFM tips,” *Bioconjug Chem*, vol. 22, no. 6, pp. 1239–1248, Jun. 2011, doi: 10.1021/BC200099T/SUPPL_FILE/BC200099T_SI_001.PDF.

[31] M. S. Read, S. V. Smith, M. A. Lamb, and K. M. Brinkhous, “Role of Botrocetin in Platelet Agglutination: Formation of an Activated Complex of Botrocetin and von Willebrand Factor,” *Blood*, vol. 74, no. 3, pp. 1031–1035, Aug. 1989, doi: 10.1182/BLOOD.V74.3.1031.1031.

[32] O. J. T. Mccarty, S. D. J. Calaminus, M. C. Berndt, L. M. Machesky, and S. P. Watson, “von Willebrand factor mediates platelet spreading through glycoprotein Ib and αIIbβ3 in the presence of botrocetin and ristocetin, respectively,” *Journal of Thrombosis and Haemostasis*, vol. 4, no. 6, pp. 1367–1378, Jun. 2006, doi: 10.1111/J.1538-7836.2006.01966.X.

[33] K. Fukuda, T. Doggett, I. J. Laurenzi, R. C. Liddington, and T. G. Diacovo, “The snake venom protein botrocetin acts as a biological brace to promote dysfunctional platelet aggregation,” *Nature Structural & Molecular Biology 2005 12:2*, vol. 12, no. 2, pp. 152–159, Jan. 2005, doi: 10.1038/nsmb892.

[34] K. Nishio, P. J. Anderson, X. L. Zheng, and J. E. Sadler, “Binding of platelet glycoprotein Ibalpha to von Willebrand factor domain A1 stimulates the cleavage of the adjacent domain A2 by ADAMTS13,” *Proc Natl Acad Sci U S A*, vol. 101, no. 29, pp. 10578–10583, Jul. 2004, doi: 10.1073/PNAS.0402041101.

[35] M. Auton, M. A. Cruz, and J. Moake, “Conformational stability and domain unfolding of the Von Willebrand factor A domains,” *J Mol Biol*, vol. 366, no. 3, pp. 986–1000, Feb. 2007, doi: 10.1016/J.JMB.2006.10.067.

[36] B. M. Luken, L. Y. N. Winn, J. Emsley, D. A. Lane, and J. T. B. Crawley, “The importance of vicinal cysteines, C1669 and C1670, for von Willebrand factor A2 domain function,” *Blood*, vol. 115, no. 23, p. 4910, Jun. 2010, doi: 10.1182/BLOOD-2009-12-257949.

[37] E. L. Bearer, J. M. Prakash, and Z. Li, “Actin Dynamics in Platelets”.

[38] M. B. Horev *et al.*, “Differential dynamics of early stages of platelet adhesion and spreading on collagen IV- and fibrinogen-coated surfaces,” *F1000Res*, vol. 9, pp. 1–27, 2020, doi: 10.12688/F1000RESEARCH.23598.2.

[39] L. Nicolai *et al.*, “Vascular surveillance by haptotactic blood platelets in inflammation and infection,” *Nature Communications 2020 11:1*, vol. 11, no. 1, pp. 1–16, Nov. 2020, doi: 10.1038/s41467-020-19515-0.

[40] L. M. M A C H E S K Y à, “Identification of a novel, actin-rich structure, the actin nodule, in the early stages of platelet spreading”, doi: 10.1111/j.1538-7836.2008.03141.x.